VTT Technical Research Centre of Finland

A New Propulsion Concept for High Propulsive Hydrodynamic Efficiency

Sanchez Caja, Antonio; Martio, Jussi; Viitanen, Ville

Link to publication

A new propulsion concept for high propulsive hydrodynamic efficiency

A. Sánchez-Caja [*], J. Martio, V.M. Viitanen

VTT Technical Research Center of Finland, Finland

ARTICLE INFO

ABSTRACT

A novel marine propulsor concept is presented for high hydrodynamic efficiency. Optimum performance is sought by thrust-producing counter-flapping foils cyclically oscillating along a closed trajectory. The thrusting device exhibits low propulsion loading and low viscous losses. In particular, the concept incorporates.

-lifting surfaces located at the ship stern with propulsive swept area larger than that of conventional propellers;

-optimum spatial distribution of axial velocities induced by the propulsor in the wake.

-elimination of transverse velocities induced by the propulsor in directions perpendicular to the ship motion;

-minimization of unsteady viscous losses compared to conventional oscillating foil concepts for thrust production.

The arrangement of lifting surfaces allows for optimum generation of a steady and uniform overall thrust over the propulsor swept area. In addition, no rudders are needed for directional motion control. Gains in efficiency relative to other propulsion concepts are estimated by potential flow theory. Significant efficiency improvements relative to other advanced propulsors like CRP, cycloidal propellers, etc. are foreseen. An URANS method is used to validate and quantify energy savings in open water conditions for a particular design case.

1. Introduction

Reduction of hydrodynamic energy losses has been a major concern in marine propulsion research during the last century. Different propulsion concepts have been proposed as alternatives to the conventional propeller with the aim of improving propeller efficiency. Generally, it is known from momentum theory that efficiency grows as propeller loading decreases. For that reason, several attempts have been made to reduce the propeller loading for a given thrust by *increasing the available propulsive area* (van Manen et al., 1997; Bose et al., 2008). For a conventional propeller, such area is dependent on the propeller diameter with a maximum size limited by the ship draught.

To benefit from the area available over the entire ship breadth, developments have been then made in two directions. Either the number of propellers to be accommodated at the ship stern has been increased (twin- or multi-screw arrangements, etc.); or unconventional propulsors of rectangular propulsive area have been proposed with working principles inspired from marine life (oscillating foils, cycloidal propellers, …). In the latter case, the performance is highly dependent on unsteady motion phenomena.

At this point, we would like to clarify a frequent misunderstanding concerning the relationship between optimum efficiency and propeller loading. Comparing co-axial multistage propulsion units (CRP, tandem, etc.) to conventional propellers of the same diameter, in principle, the individual propellers of the multistage unit would exhibit reduced loading, i.e. the "propeller" area for the unit is doubled when compared to a conventional propeller. However, such unloading does not lead necessarily to high efficiency. High efficiency is more related to what can called low "propulsive" loading/area, than to what is usually called low "propeller" loading/area. By "propulsive" area, we mean the area perpendicular to the inflow directly affected by the working propulsor.

For CRP or tandem arrangements, the propulsive area coincides with the area of the fore propeller. The fore- and aft-propellers are working under favorable conditions of reduced "propeller" loading. However, there is a detrimental interaction effect caused on the individual propeller inflows: each propeller is working under a negative effective-wake fraction caused by the action of the other propeller, which makes the benefits in efficiency of such unloading marginal or even fictitious. Low "propulsive" loading should be targeted rather than low "propeller" loading. The success of CRP arrangements lies mainly on the cancellation of rotational losses, not on the increase of the propeller area and consequent reduction of "propeller" loading. The reason is that the
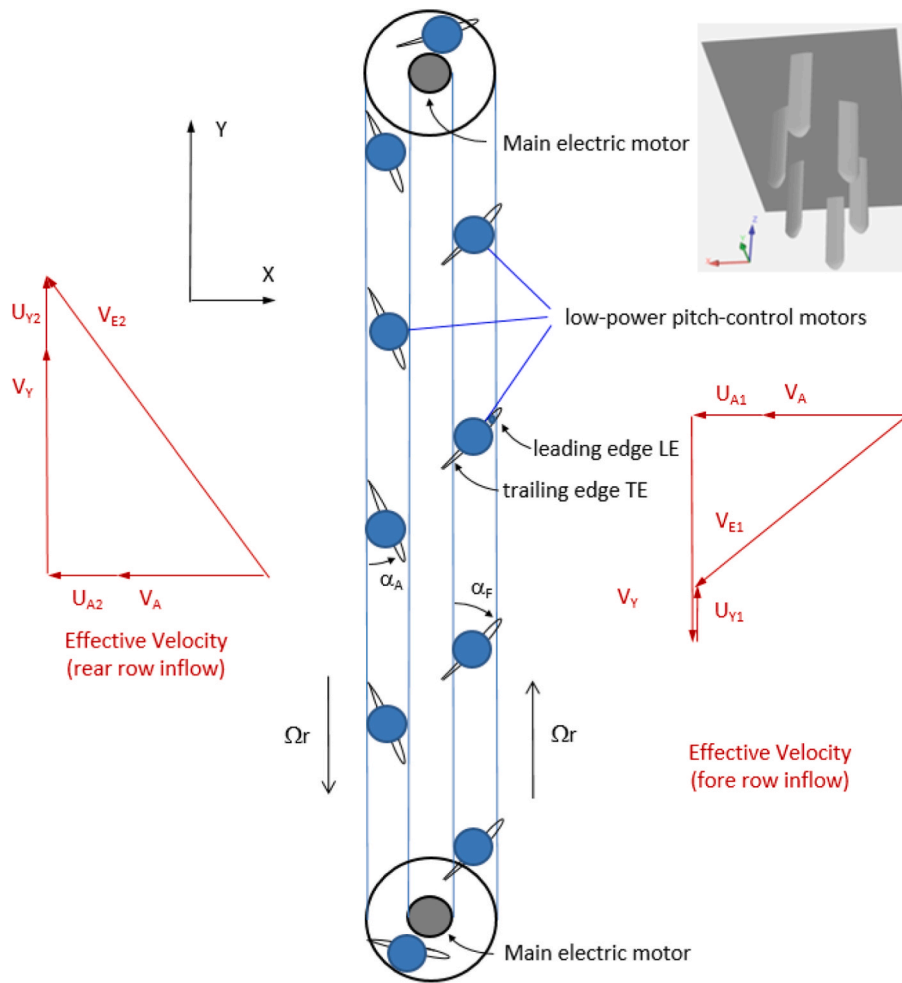

Fig. 1. Notional arrangement of lifting surfaces for the novel propulsor.

"propulsive" area of such units is not increased with respect to that of conventional propellers with the same diameter, nor are the conditions at the Treffz plane at infinity downstream modified (see Sánchez-Caja et al., 2017a for further explanation).

Furthermore, for a given fixed propulsive area, optimum efficiency should be sought by *decreasing the losses due to vortex generation,* which are directly related to the production of the so-called propeller-induced velocities. Such velocities can be generated either in the direction of the motion (e.g., axial losses for propellers) or in directions normal to the motion (e.g. rotational losses for propellers; and beam- or draft-oriented transversal losses for oscillating-foil propulsors). The latter induced velocities do not contribute to thrust production. Ideally, they should be cancelled to the maximum extent possible using adequate solutions. For example, for CRP propellers rotational losses of the fore-propeller are recovered by the action of the aft-propeller. On the contrary, the axial induced velocities cannot be completely cancelled out since otherwise no thrust would be generated by change of axial momentum in the fluid. However, axial losses can be theoretically further optimized, by producing appropriate spatial distributions of induced velocities in the propulsor wake, e.g. constant induced velocities across the slipstream for an idealized propulsor.

Other factors affecting efficiency are related to the *uniformity of the effective local inflow* associated with the propulsor concept. Note that for conventional propellers in ideal uniform axial flow, the cylindrical sections of the blades are working at local effective inflows varying radially in both magnitude and orientation, which in turn results in a radially varying sectional loading. Similarly, for foils oscillating with sinusoidal, cycloidal-like, or trochoidal trajectory motions, the lifting surfaces are working at different loading conditions over time, depending on the instantaneous angle of attack and magnitude of the local inflow. In other words, the former propulsors have kinematic inflow conditions with non-uniformity at least in *space* whereas the latter ones display non-uniformity also in *time*. Such non-uniformities are responsible for the generation of uneven frictional resistance with their associated unsteady losses; and partially responsible for the generation in the propeller wake of the so-called *free* vorticity in the former case and *shed* vorticity in the latter one using propeller-theory terminology (Kerwin and Lee, 1978). Vortex generation means energy losses. Therefore, it would be desirable for a new class of optimum propulsors to have an extent as large as possible of inflow uniformity in both time and space, which would provide operating conditions around optimum ideal performance.

This paper presents a novel propulsor concept for enhanced hydrodynamic performance (section 2). Hydrodynamic losses of different type are globally minimized by enforcing translational and rotational motions on lifting surfaces over selected foil trajectories. An ideal efficiency analysis is first presented to illustrate the potential of the new propulsor concept for efficiency improvement (section 2.1). Potential flow theory suitable for parametric optimization is used for preliminary design (section 2.2). URANS computations suitable for detailed hydrodynamic analysis are used for concept validation (section 2.3). This paper focuses on open water efficiency. The performance of the new propulsor is compared to that of a conventional propeller arrangement for a twin-screw vessel.
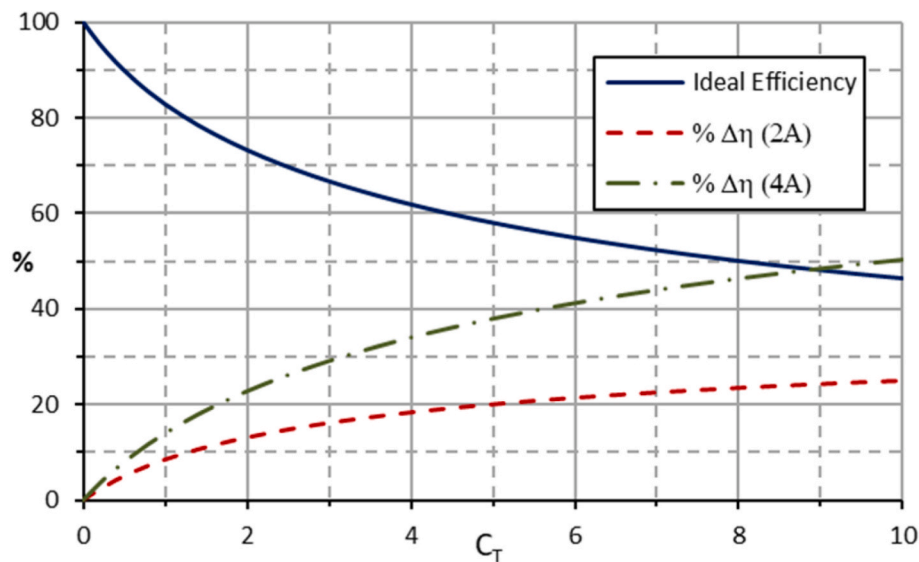
Fig. 2. Ideal efficiency and efficiency increases for double (2A) and quadruple (4A) propulsive areas as a function of the thrust loading coefficient.
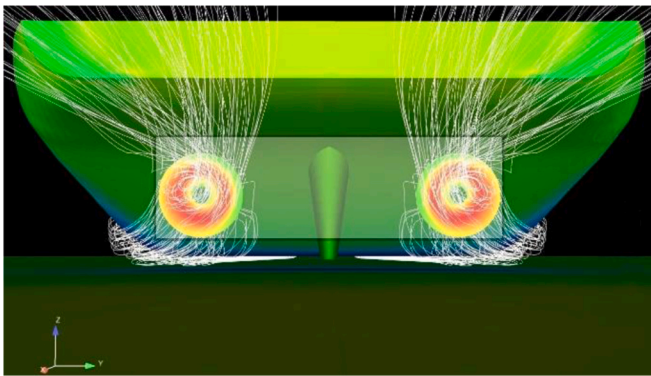

Fig. 3. Illustration of the achievable increase of propulsive area for the new propulsor concept (rectangle) compared to a twin propeller solution in a container ship. Stern view.

2. Propulsor concept

Much has been said in the scientific literature about the need to learn from nature if we want to develop efficient propulsors. Fish and marine mammal have been inspirational to scientists to seek new and more efficient ways of marine locomotion. Some examples are foils oscillating in pitch and heave that have been extensively studied theoretically (see e. g., Lighthill, 1975; Wu, 1961, 1971; and more recently Belibassakis and Politis, 2013) and experimentally (Scherer, 1968; DeLaurier and Harris, 1982; Lai et al., 1993; Triantafyllou et al., 2000, 2004; Taylor et al., 2003; Vermeiden et al., 2012). Other examples are, pulsing jet motions (Krieg and Mohseni, 2017), and manta ray swimming (Smits, 2016). On the other hand, human inventions can go beyond limitations of living organisms in the search of efficient propulsion solutions since artificial thrusting devices are not limited by living-body constraints.

The novel propeller concept is based on an endless-chain/belt mechanism for foil motions where unsteady phenomena are confined to a small portion of the trajectory (Fig. 1). A motor rotating with angular speed Ω activates the mechanism. Foils move perpendicular to the direction of the inflow V_A, being arranged in two parallel rows traveling in opposite directions at speed V_Y equal to $\Omega.r$, being r the radius of the circular trajectories at the edges. On the one hand, the foils located in the downstream row benefit from the velocities induced by the foils in the front row, recovering in this way lateral losses in the

direction perpendicular to the vessel motion. On the other hand, losses due to unsteadiness (shed vortices) are reduced over those present in flapping mechanisms, since they are produced only at the edges of the row. In this way, a uniformity of local inflow in time and space over most of the trajectory is achieved.

The mechanism is capable of producing uniform distribution of axial thrust (spatial optimization of axial induced velocities), avoiding lateral losses (cancellation of transversal induced velocities), and minimizing unsteady losses (low unsteady vortex shedding). The concept allows a large uniformity of inflow in space and time over most of the foil trajectory, and therefore, the foils operate at optimum conditions of lift production as well as of frictional and induced drag reduction.

Devices with similar working principles can be found in turbines (Minaki H., 2013; Beaudoin N., 2013; Syrovy G. J., 2011) and aircraft (Vetter, 2013; Steiner, 2002) patents. However, they require the use of either bi-symmetric camber and thickness distributions to allow for rear effective inflow (trailing edge inflow) over portions of the foil paths, or conventional symmetric profiles moving at velocities larger than the operational ship speed as is the case of Voith Scheneider (VS) propellers. In the latter case, high foil velocities avoid rear effective inflow to the foils, but penalize efficiency and increase the risk of cavitation. In addition, such devices (except VS propellers) have not been proposed for marine propulsion applications.

2.1. Efficiency

The use of large area propulsors increases the levels of attainable ideal efficiency far above those of conventional propellers. Fig. 2 shows the increments in ideal efficiency that can be achieved by doubling and quadrupling the propulsive area of a propulsor. For loading coefficients around and above 0.5–1, huge improvements in efficiency are expected.

Increases in propulsive area between twice and thrice are easily achievable as shown in Fig. 3 for the case of a container ship with twin propellers.

To investigate realizable open-water improvements in hydrodynamic efficiency for the new propulsor concept, potential flow theory (section 2.2) combined with drag corrections for viscous effects is employed for parametric optimization, and an URANS viscous flow methods (section 2.3) is used for validation.

2.2. Potential flow model

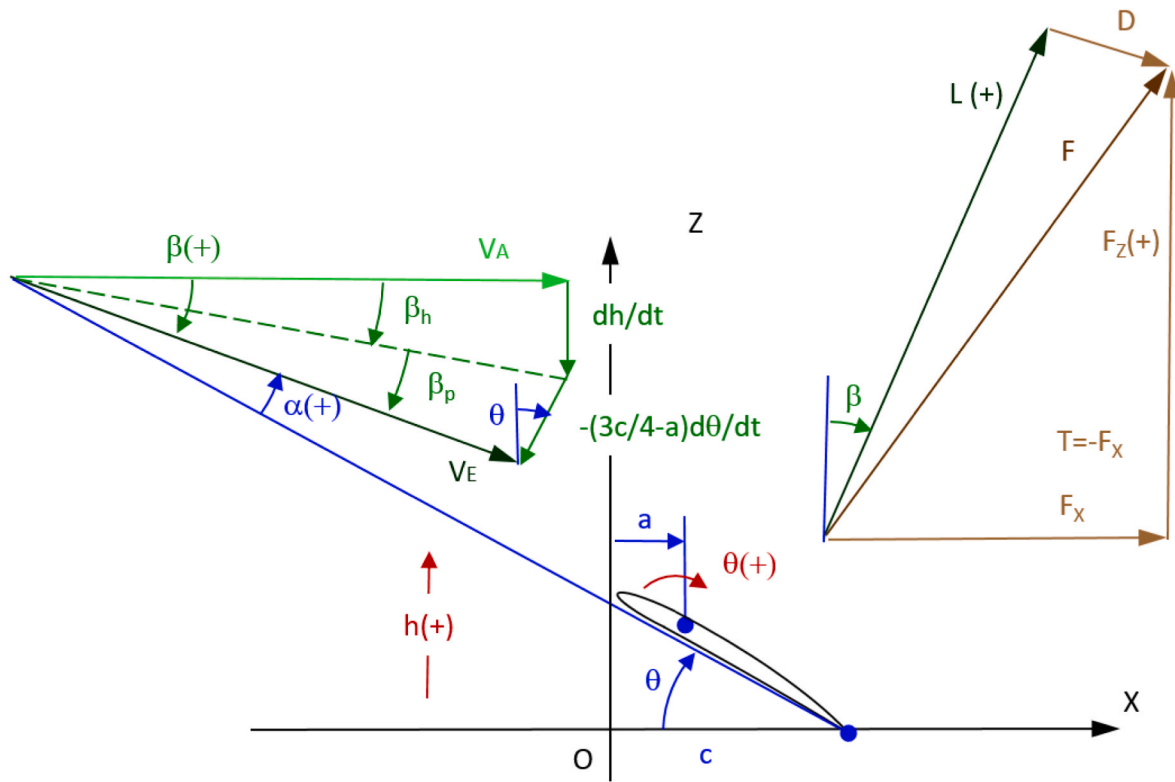The potential flow model in Sanchez-Caja and Martio (2017b) for

Fig. 4. Notional illustration of oscillating foil motions (ref. Sanchez-Caja et al., 2017).

Table 1

Comparison of main dimensions and performance coefficients for the propulsors.

	Conventional	Unconventional
No. of propellers	2	1
Diameter (m)	3	
Span (m)		4
Length (m)		11.333
chord (m)	1.01	0.90
foil pitch (deg)		65.5, 63.3
Thrust (kN)	2 × 170	340
Propulsive Area (m2)	14.14	45.33
CT	0.518	0.162

oscillating foils and cycloidal propulsors is used here with small modifications to account for the more steady-state nature of the flow along the length of the new device. The approach has been successfully applied to the performance prediction of oscillating foil propulsors in the optimum efficiency range. A short summary of the method in the reference is given in this section adapted to the new propulsor.

The foil is approximated as a flat plate. Unsteady effects are limited to a small part of the foil trajectory at the lateral edges of the propulsor. Added mass (non-circulatory) effects are modeled assuming that the foil behaves like a flat plate heaving and pitching. Three-dimensional effects on lift and drag coefficients are modeled according to lifting line wing theory with corrections based on tests with rudders. Drag and lift breakdown are simulated assuming a standard behavior for angles larger than the stall angle. The stall angle can be estimated by an empirical equation based on thickness to chord ratio or given as an input.

Fig. 4 shows the nomenclature used in this section for the individual foil analysis. As the foil is moving with a chain-like motion in a ship frame of reference, the trajectory consists mainly of a lateral translation h (either up/downward vertical or right/left horizontal), and a pitch rotation θ about a pivot point at the edges in the presence of a horizontal nominal inflow V_A. The pivot point is located at a distance a from the

leading edge. The h parameter is related to V_Y in Fig. 1. V_Y is in fact $\dot{h}$ on the rectilinear portions of the trajectory, although it may include an additional constant value for oblique inflows.

The foil has a chord c and a span s. Due to the foil motions, the instantaneous angle of attack α of the relative inflow V_E to the foil is a function of flow angle β, which in turn consists of two components, one due to the translational motion (β_h) and the other due to the pitch rotation (β_p). The period of the motion T_0 is

$$T_0 = \frac{l_c}{\Omega r_0} \tag{1}$$

where l_c is the chain length, Ω is the angular speed of the wheel and r_0 the wheel radius. The pitch angle is constant over most of the straight paths with different signs depending on the direction (upward or downward). A circulatory lift L perpendicular to the relative inflow and a viscous drag D in the direction of the relative inflow are generated. The projection of these forces on the direction of motion contribute to the production of thrust for $\beta > \theta$ (or $\alpha < 0$), and their projection on the vertical direction, to a vertical force F_Z responsible for power consumption. Note that Fig. 4 is presented as such only for illustration purposes on the nomenclature, but in a real application the angle β should be larger than θ in order to have a positive thrust ($T = -F_x$) in the x-direction.

An additional lift L_{AM} due to added mass will be present acting on the vertical direction (Katz and Plotkin, 1991). The circulatory 2D lift L and added mass lift can be expressed as

$$L = \pi \rho V_A^2 c C(k)[\theta - \beta] \tag{2}$$

$$L_{AM} = \frac{1}{4} \pi \rho c^2 \left(V_A \dot{\theta} - \ddot{h} + \left(\frac{c}{2} - a \right) \ddot{\theta} \right) \tag{3}$$
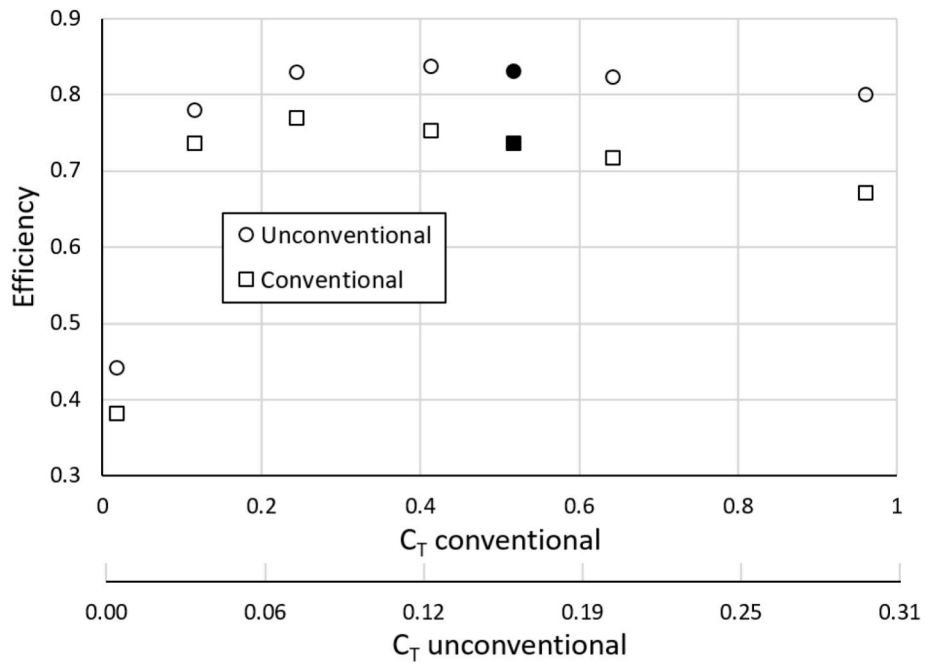
Fig. 5. Comparison of performance between the two propulsors for constant overall thrust at design (filled markers) and off-design (non-filled ones) conditions.
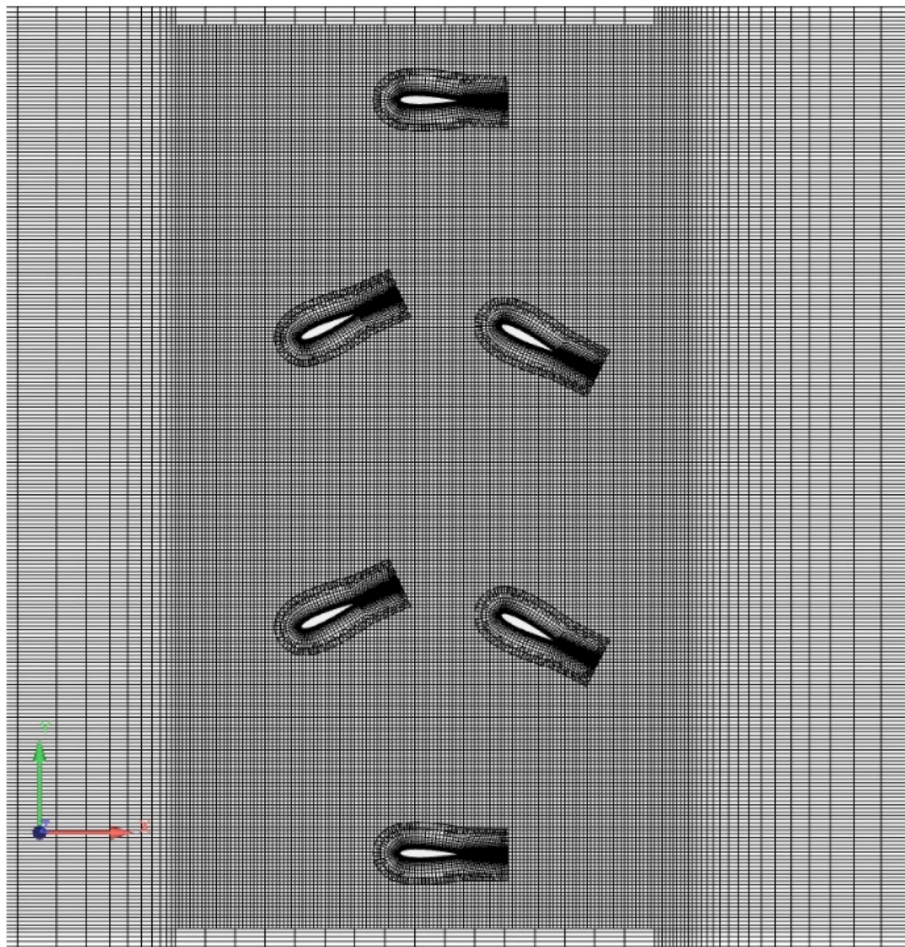

Fig. 6. Two-dimensional grid for the novel propulsor. The Chimera and background blocks are visible.
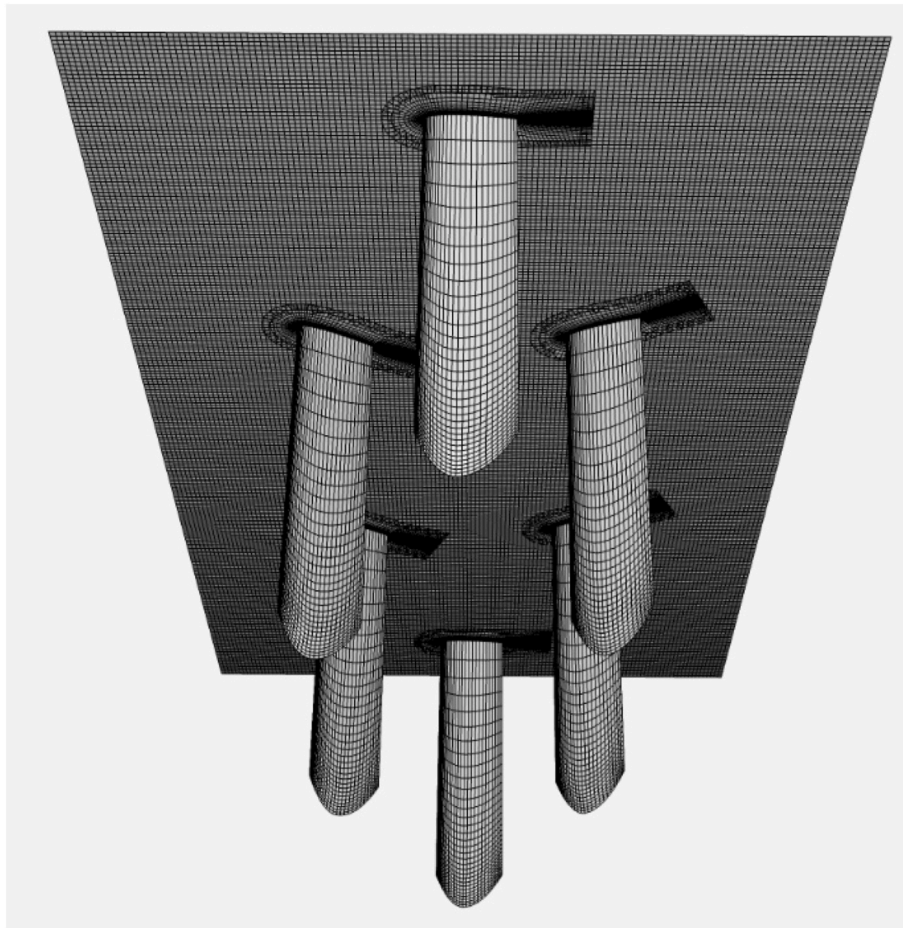
Fig. 7. Three-dimensional grid for the novel propulsor. The Chimera blocks are visible on their solid surfaces.

Table 2
Comparison of forces for original and fine grids for the 2D case.

	URANS	URANS	DF/FTOTAL
	initial grid	fine grid	Δη
J	1.25	1.25	
T (kN)	378	387	2.3%
Fy (kN)	−97	−54.5	10.9%
FTOTAL (kN)	390	391	0.1%
η	0.905	0.902	0.3%

$$\beta = \arctan \left[\frac{-V_Z + \dot{h} - \dot{\theta}\left(\frac{3}{4}c - a\right)\cos\theta}{V_A + \dot{\theta}\left(\frac{3}{4}c - a\right)\sin\theta} \right]$$

Similarly, a circulatory moment Q and an added mass moment Q_{AM} are given as

$$Q = \frac{\pi}{4}\rho c^2 \left(\frac{4a}{c} - 1\right) V_A^2 C(k)[\theta - \beta] = Lc\left(\frac{a}{c} - \frac{1}{4}\right) \tag{4}$$

$$Q_{AM} = -\frac{\pi\rho c^2}{4} \left[\begin{array}{l} \left(a - \frac{c}{2}\right)\ddot{h} + \left(\frac{3}{4}c - a\right)V_A\dot{\theta} \\ +\frac{c^2}{4}\left(\frac{9}{8} + \frac{4a^2}{c^2} - \frac{4a}{c}\right)\ddot{\theta} \end{array} \right] \tag{5}$$

where V_Z is a possible vertical (or lateral) inflow which will be assumed zero, ρ is the fluid density and $C(k)$ is Theodorsen's complex function

accounting for the unsteady wake effect in the form of a lift deficiency factor and phase lag. As the unsteady effects are confined to a small portion of the trajectory at the edges, the function will be assumed to be constant and equal to one in this study.

The variation of pitch angle and foil translation over time are represented by Fourier series. The harmonic oscillations can be expressed in complex form,

$$h = \sum_n h_{0n} e^{i(n\omega t - \pi/2)} \qquad \theta = \sum_n \theta_{0n} e^{i(n\omega t + \psi - \pi/2)} \tag{6}$$

And the effective attack angle can be decomposed by Fourier series,

$$\theta - \beta = \sum_{n=1,N} A_n e^{i(n\omega t - \pi/2)} + \sum_{n=0,N} B_n e^{i(n\omega t)} \tag{7}$$

The 3D thrust T, vertical force F_Z and moment about the pivot point Q_{OY} are calculated as follows,

$$F_Z = \overline{L}\cos(\beta) - \overline{D}\sin(\beta) + L_{AM}s \tag{8}$$

$$-T = F_X = \overline{L}\sin(\beta) + \overline{D}\cos(\beta) \tag{9}$$

$$Q_{OY} = \overline{Q} + Q_{AM}s \tag{10}$$

Here $\overline{L}, \overline{D}, \overline{Q}$ means 3D circulatory lift, drag and torque. In order to account for 3D effects, following lifting line theory, the circulatory terms in (2) can be expressed in the form

$$\overline{C}_L \approx \frac{2\pi(\theta - \beta)A}{(A + 2)} \qquad \overline{C}_L \approx \frac{1.95\pi(\theta - \beta)}{(1 + 3/A)} \tag{11}$$

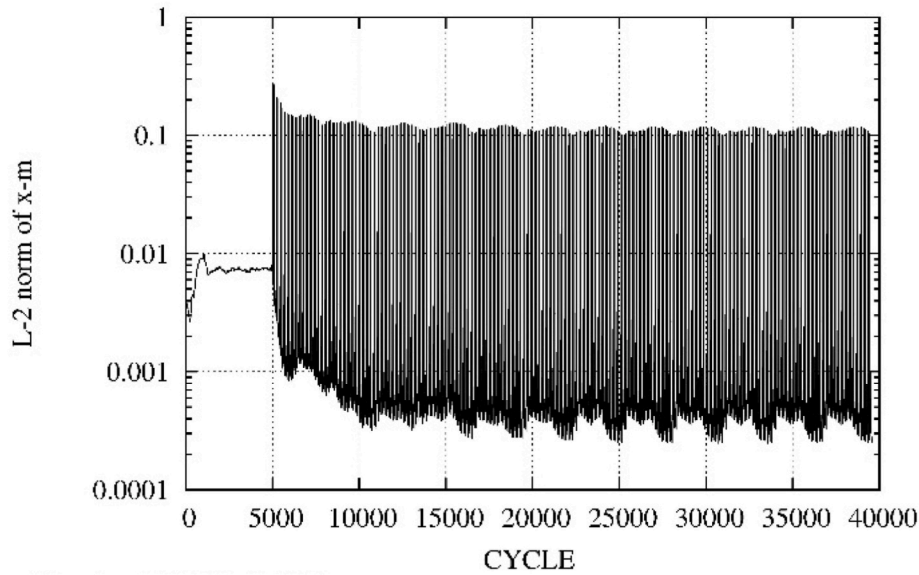The equation on the left is the theoretical lift for an optimum wing of

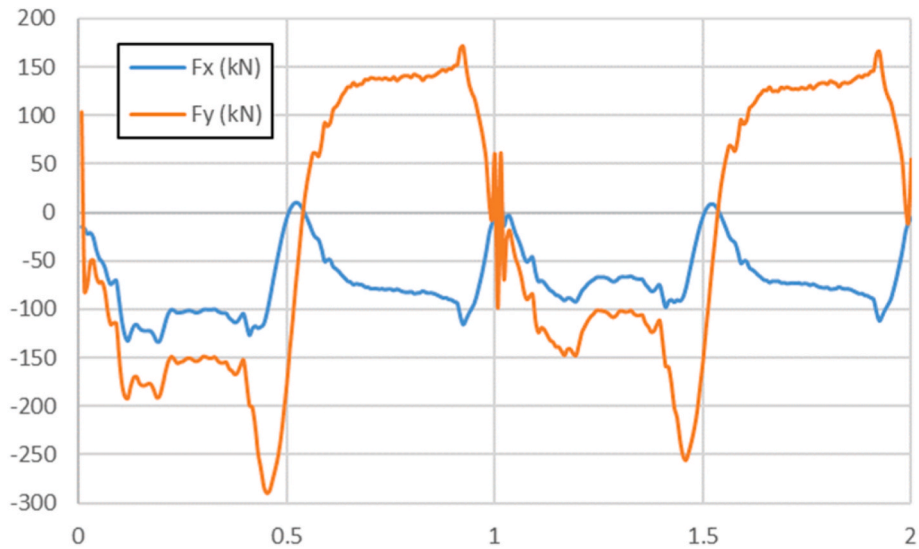**Fig. 8.** Convergence history of momentum residuals for the 3D case.

Fig. 9. Evolution of forces over the two first time cycles for a single blade. 3D URANS simulation. Convergence is reached after one cycle.

aspect ratio A in uniform flow at an angle of attack $\theta - \beta$. The equation on the right is an alternative formulation suggested by Molland and Turnock (2007) which represents a satisfactory mean line through available rudder data. The latter is used in this work. Recourse to such simplified modelling is common in other related areas like ship motion control simulation (e.g. Matusiak and Rautaheimo, 2017).

An additional correction to the inflow is implemented in the calculation inspired in propeller lifting line theory. The thrust and lateral forces induce axial and lateral velocities that should be added to the inflow for the estimation of effective angles of attack. The induced velocities have been estimated by momentum theory, e.g.\

$$U_A = \frac{V_A}{2}\left(-1 + \sqrt{1 + C_T} \right) \tag{12}$$

where C_T is the thrust load coefficient based on the propulsive area, i.e. the area swept by the foil.

Analogously, the overall drag coefficient can be calculated as follows,

$$\overline{C}_D = \frac{\overline{C}_L^2}{\pi e A} + \frac{\overline{D}_0}{0.5 \rho V_E^2 S} \tag{13}$$

The first term is the induced drag, which results from lifting line analysis of optimum wings with aspect ratio A, and the second one is a frictional drag. The efficiency factor e is introduced into the induced drag term to bring predictions using the drag equation in line with the experimental data.

The effective (PE) and delivered (PD) power are calculated as follows,

$$PE = TV_A \quad PD = -F_Z\dot{h} - Q_{PY}\dot{\theta} \tag{14}$$

and the efficiency,

$$\eta = \frac{PE}{PD} \tag{15}$$

Sanchez-Caja et al. (2017b) provides more details about the method, including topics like how lift breakdown and drag after stall are
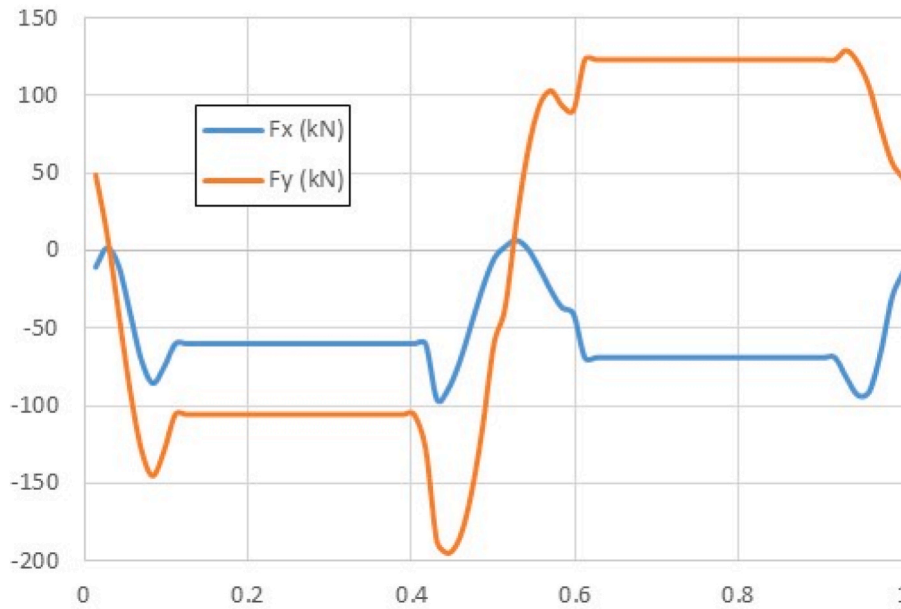
Fig. 10. Evolution of forces over a time cycle for a single blade. Potential flow simulation.

Table 3
Performance predictions for the new and conventional propellers for the 3D case.

	Potential flow	Potential flow	Viscous flow
	Conventional	Unconventional	Unconventional
J	1.05	1.25	1.25
T (kN)	2 × 170	340	342
Fy (kN)	0	0	−33
η	0.737	0.831	0.832

modeled, how the circular motion of the foils at the edges can be treated (i.e. like in cycloidal propellers) and how parameter optimization can be performed. In this particular study, the optimization target was finding the motor RPM and foil pitch angles for a given thrust, zero overall lateral force and minimum delivered power.

2.3. VISCOUS flow model

The flow simulation is made with RANS solver FINFLO. A description of the numerical method including discretization of the governing equations, solution algorithm, etc. can be found in Sanchez-Caja et al. (1999). The solution of the RANS equations is obtained by the pseudo-compressibility method. The momentum equations can be written in the following form

$$\rho \frac{D\overrightarrow{V}}{Dt} + \nabla p - \mu \nabla^2 \overrightarrow{V} = \rho \overrightarrow{g} + \overrightarrow{F}_{AD} \tag{16}$$

where $\overrightarrow{V}$ is the velocity vector, ρ is the density, μ is the dynamic viscosity, $\overrightarrow{g}$ the acceleration of gravity and $\overrightarrow{F}_{AD}$ possible body forces. The equation can be expressed in terms of a vector U of conservative variables $(\rho, \rho u, \rho v, \rho w, \rho k, \rho \varepsilon)^T$, where u, v and w are the absolute velocity components; k is the turbulent kinetic energy and ε is the dissipation of k.

FINFLO solves the RANS equations by a finite volume method. The implicit solution is based on approximately factorized time-integration with local time-stepping. In the present incompressible case, the code uses an upwind-biased approximation for convective fluxes, a Rhie and Chow type method is implemented in the code in the simplified form

presented by Johansson et al. (1995). The pressure is central-differenced and a damping term is added via a convective velocity. For the time derivatives, a second-order three-level fully implicit method is used. The viscous solution is extended to the wall and SST k-omega turbulence model was used in the simulations.

Validation of the FINFLO code with experiments has been provided over the years for a wide range of propeller types like pod units, ducted propellers, tip loaded propellers, CRP units, flapping foils and cycloidal propulsors, etc. (e.g. Sánchez-Caja et al., 1999, 2000, 2014, 2017, 2018, respectively) resulting in good estimations of performance coefficients.

Special boundary conditions are used for modeling the translating and pitching motions of the individual foils. Overlapping grids (Chimera blocks) are used describing prescribed foil trajectories with wall velocities enforced on the solid surfaces. Mirror boundary conditions were applied to the foil on the root plane in the 3D case.

The effective and delivered power are calculated by integrating and averaging the forces over one cycle as follows,

$$PE = \frac{Z}{l_c} \oint \overrightarrow{V}_S \cdot \overrightarrow{F} ds = -\frac{ZV_A}{l_c} \oint F_x ds$$

$$PD = -\frac{Z}{l_c} \left(\oint \Omega r_0 \overrightarrow{F} \cdot d\overrightarrow{s} + \dot{\theta} \cdot \overrightarrow{Q} ds \right) \tag{17}$$

where Z is the number of blades, $\overrightarrow{F}$ is the blade force and $\overrightarrow{Q}$ is the blade moment around a pivot point for a foil describing a closed trajectory C, $d\overrightarrow{s}$ is a path differential over the trajectory, $\overrightarrow{V_S}$ is the ship speed, Ωr_0 is the local linear speed of the foil in the propulsor frame of reference, and $\dot{\theta}$ is the angular speed around the pivot point. Equation (15) provides the efficiency.

2.4. NON-DIMENSIONAL coefficients

For the non-dimensional analysis of conventional propellers, the usual parameters are the advance coefficient J for kinematic similarity, a scale factor for geometric similarity, Reynolds and Froude number for dynamic similarity of inertial to viscous and gravity forces, respectively. Additionally, other parameters such as the pitch diameter ratio P/D, the expanded area ratio A_E/A_0 and the number of blades Z affect the forces, which are usually represented in graphical form in terms of thrust and torque coefficients, K_T and K_Q. Alternatively, the thrust loading and power coefficients C_T and C_P can be used.
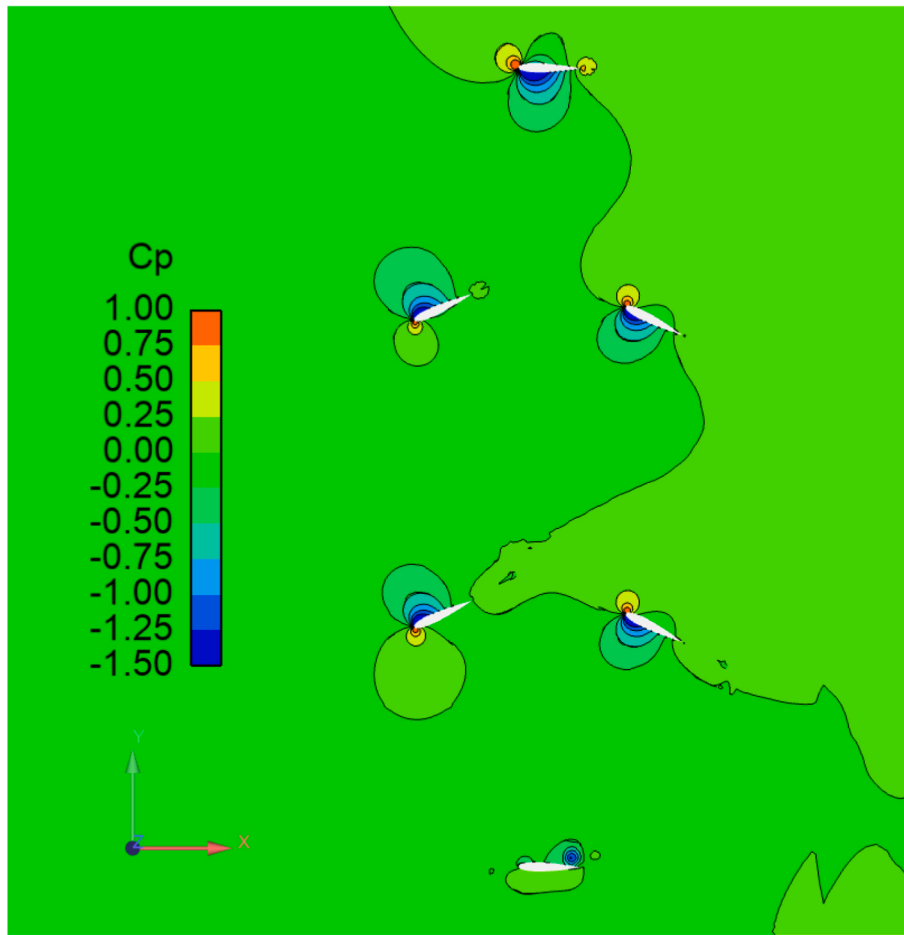
Fig. 11. Distribution of pressures around the propulsor. An underpressure and an overpressure are visible upstream and downstream of the propeller, respectively.

Similar parameters can be used for the new propulsor. The advance coefficient may include, instead of the propeller diameter *D* and revolutions per second *n*, the diameter of the edge wheels and the rotation rate of the wheels. Their product represent the lateral velocity of the foil rows in the new propulsor similar to the circumferential velocity in the propeller case.

Additionally, the foil angle at the fore row may be used as representative parameter of the pitch diameter ratio in propellers. The angle at the aft row can be considered dependent on the fore one, having a magnitude such that the lateral force is cancelled around optimum operation.

Contrary to the propeller case, two parameters define the propulsive area, the foil span *s* and propulsor transversal length *l*. Then, an additional parameter, the *propulsive-area aspect ratio s/l,* can be introduced which will affect performance for a given propulsive area. Besides, the expanded area will be *cZ/l,* being *c* the foil average chord.

For oscillating foil propulsors, due to the dominant character of unsteady phenomena in thrust production, additional non-dimensional parameters are introduced, e.g. the Strouhal number *St* and the reduced frequency *k* (Anderson et al., 1998). Here, we can define for example the Strouhal number in terms of the transversal length of the propulsor *l*, the period of the motion T_0 and the inflow velocity *V*,

$$St = \frac{l}{T_0 V} \tag{18}$$

This parameter would be relevant to our study only for devices of small length, but in such cases, we would be changing from the proposed propulsor concept to another one that looks like a cycloidal propeller, and therefore we would lose the main benefits of steady thrust

production over the rectilinear rows of the novel concept. For that reason, such propulsor lengths are not considered relevant.

3. Study case

In this section, the main design parameters of the new propulsor for a case study are compared to that of a conventional propeller belonging to a notional twin-screw vessel sailing at 18.5 knots. The alternative designs are made for a given overall thrust.

Table 1 shows the main dimensions and input data for the conventional and new propulsors. NACA 0015 profiles are selected for the blades of the unconventional propulsor.

Potential flow theory in section 2.2 and standard lifting line theory provides the performance estimations for the new and conventional propeller, respectively. The design loading is $C_T = 0.518$ for the conventional propeller, which corresponds to $C_T = 0.162$ for the new propulsor. Fig. 5 compares the performance of the new propulsor to that of the twin conventional propellers at different loading conditions. The horizontal axis provides the C_T coefficients for the conventional (upper axis) and unconventional (lower axis) propulsor. Each vertical line corresponds to an operation point of constant overall thrust, being the loading coefficient smaller for the unconventional propulsor. The filled makers in the figure are for the design condition. The analysis of the conventional propeller was made for different axial inflows at constant rpm (corresponding to the design point), covering relevant advance numbers. As the unconventional propeller can freely change the blade pitch, the blade pitch and revolutions have been optimized for each speed and thrust level of the conventional propeller enforcing zero lateral force.
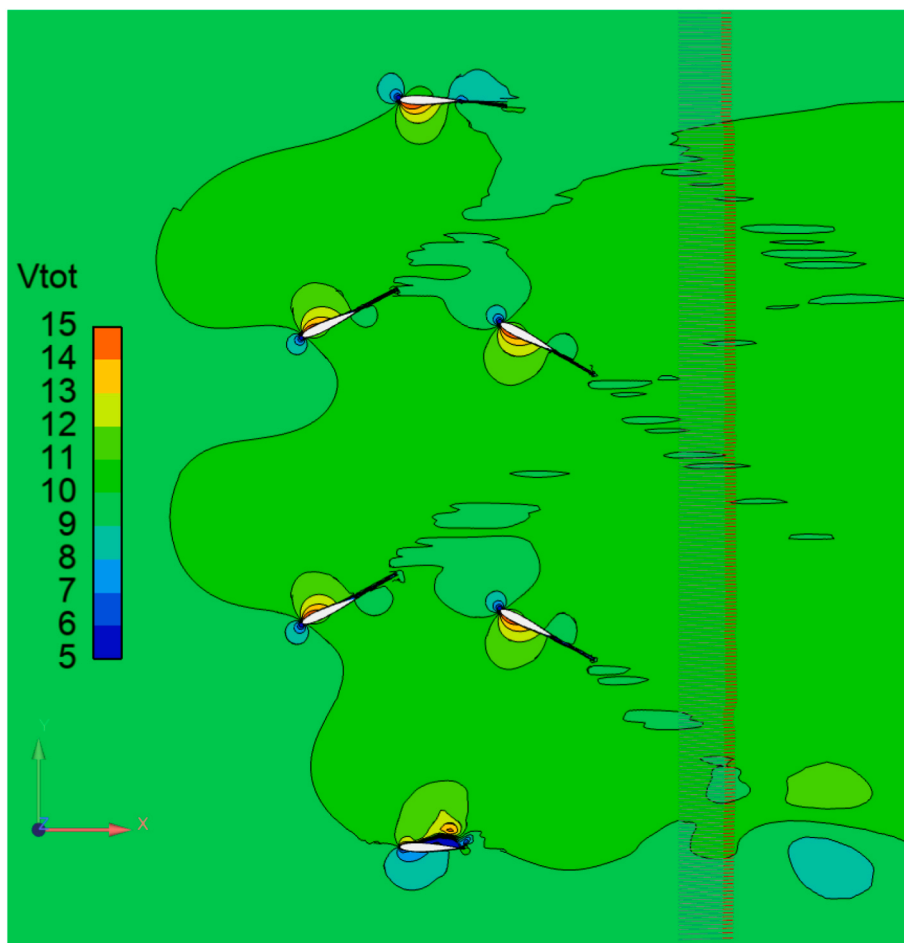
Fig. 12. Distribution of total velocities around the propulsor on the propeller wake at one time instance. The direction of the outflow is shown as red-tipped arrows on the right side. A smooth and uniform perturbation is apparent in the direction of ship motion. 2D flow. (For interpretation of the references to colour in this figure legend, the reader is referred to the Web version of this article.)

3.1. Flow analysis

To validate the performance prediction in the previous section, an URANS analysis is made for the new propulsor in open water. Figs. 6 and 7 show the computational meshes used for the validation in two-dimensional (2D) and 3D flow, respectively. The 2D arrangement shown in Fig. 6 was identical to that used in the 3D case. The mesh differences were in the foil span direction: the 2D mesh consist of only one cell layer whereas the 3D mesh contains 88 layers for the background grid and 32 cells in the span direction of the foils in the Chimera block. The size of the meshes were about 75000 cells for the 2D case and 5.5 million cells for the 3D case. The Chimera blocks have C topology with 96 cells in the direction around the foil.

The grid size and cell distributions were chosen based on previous experience. The y^+ parameter was around one. A fine grid was built by doubling the number of cells in the grid directions to check grid convergence in 2D. The differences in the force components in the thrust and lateral directions were 2.3 and 10.9 percent, respectively. However, the difference in total forces and efficiency between the grids was very small below 0.5 percent, which is considered acceptable especially for efficiency assessment (see Table 2).

Fig. 8 shows the convergence of the momentum residuals for a sample case. The computation starts in steady-state mode and shifts after 5000 iterations to unsteady mode. A drop of the residuals of about three orders of magnitude is achieved along 300 time steps covering two overall foil cycles (i.e. twelve blade passing cycles).

Fig. 9 shows the evolution of axial and lateral forces for a single foil.

The foil transit in pitch from the front to the rear row path at the low edge has been smoothed to avoid force peaks in the lateral forces. However, the transit from rear to front at the top edge is linear and presents a downward peak.

Fig. 10 shows the evolution of axial and lateral forces for a single foil as predicted with the potential flow method. The qualitative and quantitative correlation between the two methods is good.

Table 3 shows the performance predictions by potential flow theory with empirical correction for viscous effects and by viscous flow computations for the new propulsor as well as the prediction for the original conventional propeller. The correlation is good for the efficiency and thrust. Some differences are found in lateral force. The increase in open water efficiency for the novel propulsor relative to the conventional one is 13 percent. The propulsive area (Table 1) is increased about 3.2 times. Then from Fig. 2, about 6.5 percent increase corresponds to a change in ideal efficiency due to the augmented propulsive area, and the rest will be due to cancellation of lateral losses and losses related to non-uniform effective inlet and outlet flow.

Fig. 11 presents the pressures p around the propeller in terms of the pressure coefficient $C_P = 2(p-p_0)/\rho V^2$, where p_0 is the pressure at infinity, V the inflow and ρ the density. Low pressures in front and high pressures behind the propulsor are shown. The smooth pitch transition from the front row to the rear one at the lower edge results in low-pressure peaks. Conversely, the sharper linear transition at the upper edge from the rear row to the front one results in a high-pressure peak affecting the lateral force. The jump from low pressures upstream to high pressures downstream of the propeller is typical of propulsor
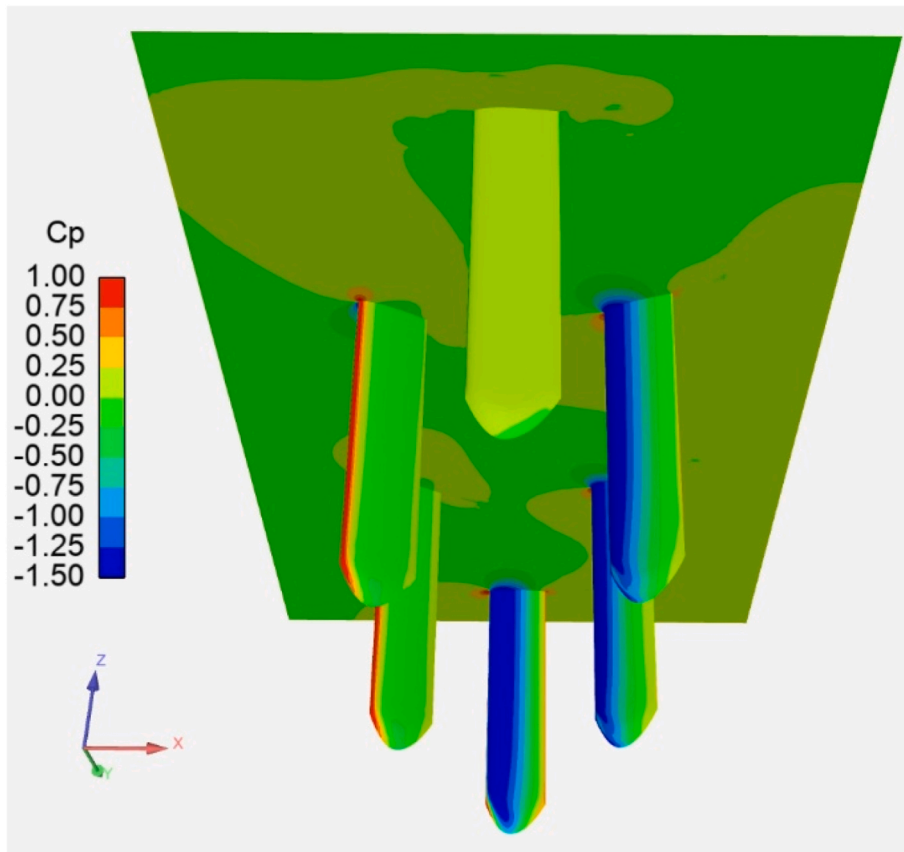
Fig. 13. Distribution of pressures around the propulsor at one time instance. 3D flow. Upstream and downstream to the left and right, respectively.
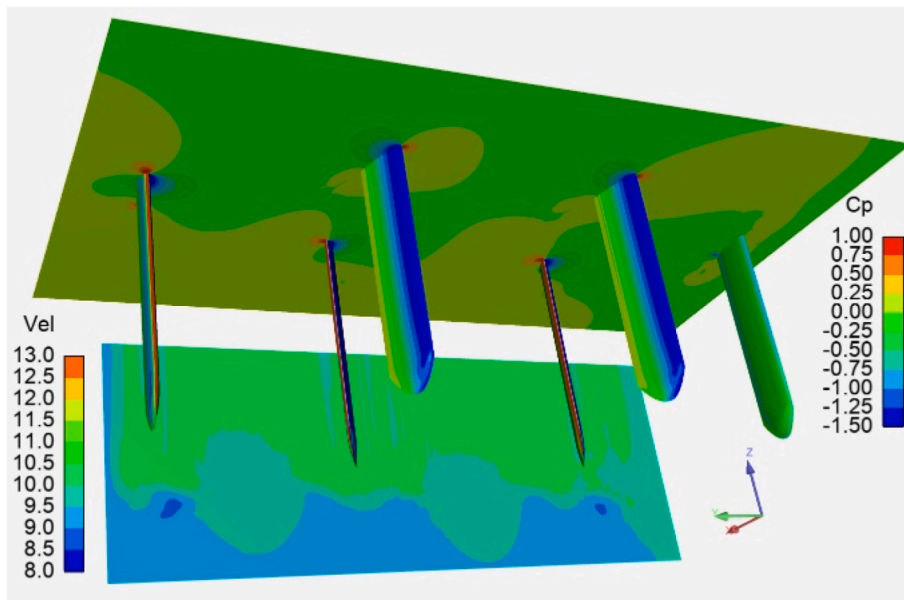

Fig. 14. Distribution of total velocities around the propulsor on the propulsor outlet plane at one time instance, x/D = 1.3. Pressures are visible on the foil surfaces and on the foil root plane. 3D flow.

devices.

Fig. 12 illustrates the natural way in which the novel propulsor concept efficiently distributes the induced velocities for thrust production. The velocity contours and velocity arrows at the outlet show a uniform, almost constant, increase in the velocity vectors along the propulsor slipstream at the outlet, without lateral flow components.

Figs. 13 and 14 show the corresponding results for the 3D case. The pressure distributions on the blade surfaces and propeller root plane are visible as well as the velocity distribution at a plane located downstream of the propulsor center at $x/D = 1.3$ for the latter figure. A uniform increase of the flow velocities on the downstream plane in the wake can be seen with a relatively smooth transition to the unperturbed inflow at
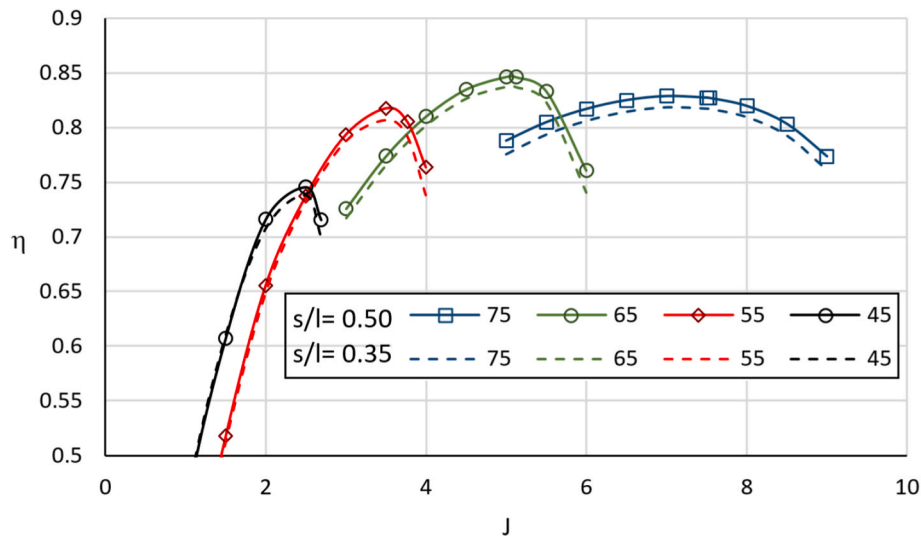
Fig. 15. Open water efficiency diagram of the novel propulsor in terms of the advance coefficient (J) and the foil angle in the front row (45–75 deg. curves). Curves for two aspect ratios of the propulsive (s/l) area are given. $A_E/A_0 = 0.48$.

Fig. 16. Thrust coefficient (C_T) diagram of the novel propulsor in terms of the advance coefficient (J) and the foil angle in the front row (45–75 deg. curves). Curves for two aspect ratios of the propulsive (s/l) area are given. $A_E/A_0 = 0.48$.
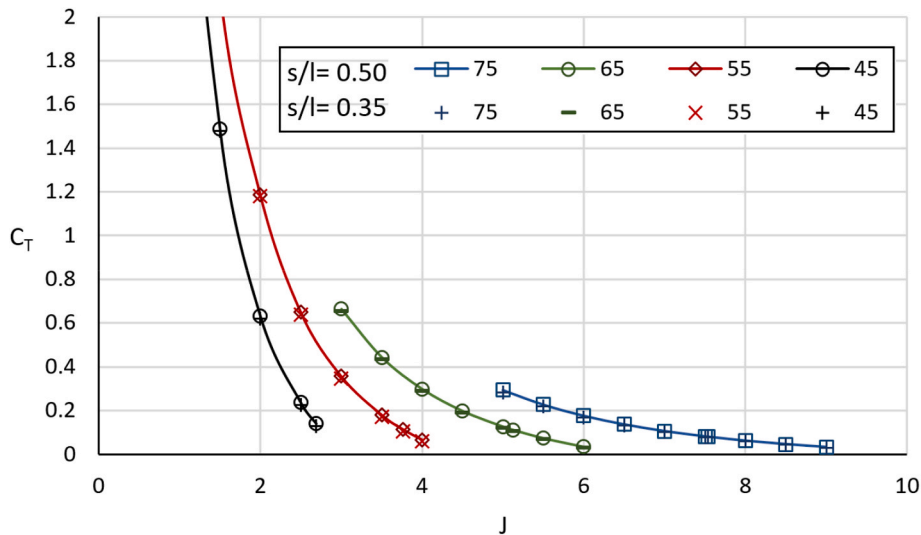
the blade tips and lateral edges.

4. Discussion

Diagrams of efficiency and C_T versus advance number and fore foil angle are shown in Figs. 15 and 16 respectively, for a constant expanded area ratio of 0.48. Two geometric aspect ratios s/l of the propulsive-area (0.35 and 0.5) are considered. The effective aspect ratios are doubled relative to the geometrical ones due to the wall plane effect at the foil roots. The curves are obtained using the potential flow theory with empirical corrections for viscous flow described in section 2.2.

The diagram in Fig. 15 reminds open water diagrams typical of conventional propellers for different pitch ratios. The difference is that the maximum attainable efficiency is much larger. In addition, contrary to conventional propellers, one single device is able to operate in the entire spectra of pitch angles with the blade sections adjusted to the optimum angle of attack, which cannot be achieved with conventional propellers even of controllable pitch (CPP) type. For CPP, the blades operate at optimum incident flow angle conditions only at the design point.

Efficiency increases with the aspect ratio of the propulsive area, and so does the thrust coefficient. The magnitude of the thrust coefficients for an equivalent conventional propeller case would be 3–4 times larger as shown in the comparative scale in Fig. 5.

In principle, the new propulsor is conceived to operate in off-design conditions by adapting the foil pitch angle to achieve the required force in magnitude and direction. Contrary to CPP propellers, the effective inflow at the sections along the span will not present strong variations in angle of attack. No rudders are required for course keeping and ship maneuvering since lateral forces can be easily generated and controlled by changing the pitch in the fore and aft foil rows. In this respect, a significant reduction in appendage resistance is easily foreseen in some propulsor configurations.

In our opinion, many efforts to improve the performance of propulsion concepts based on oscillating foils have gone in marginal directions since the research has been focused mainly on low Reynolds number flows for small vehicles while the most relevant area of interest in marine applications is operation at high Reynolds numbers. In principle,

optimization at low scales should be based on different grounds than that at large scales, being for the former case laminar separation a major physical phenomenon to be accounted for, together with its associated vortex-shedding control. However, at large scales the emphasis should be placed on minimizing overall viscous losses including unsteady vortex generation. In this way, optimum operation is not dependent on phenomena appearing at laboratory conditions difficult to control in actual full-scale applications.

5. Conclusion

A novel propulsor of high hydrodynamic efficiency has been proposed. Open water efficiency gains around 13% were found for an application of the novel propulsor to a twin-screw vessel. The efficiency increase is due not only to a large propulsive area swept by the foil blades but also to the minimization of viscous losses of steady and unsteady nature and to enhanced thrust directionality. The factors contributing to efficiency gains are generic, applicable to a wide range of vessel types.

Considerations about the propulsor concept are given from the standpoint of non-dimensional analysis. One additional non-dimensional parameter relative to conventional propellers is required for defining performance at a given propulsive area since constant area can be achieved at different foil-span to propulsor-length ratios.

Potential flow theory with empirical corrections to account for viscous flow phenomena, and URANS computations have been made for concept validation from a hydrodynamic point of view. The focus was on performance in open water conditions. Future work will include studies on ship performance in behind condition.

CRediT authorship contribution statement

A. Sánchez-Caja: Conceptualization, Data curation, Formal analysis, Writing – original draft. **J. Martio:** Conceptualization, Formal analysis, Writing – review & editing. **V.M. Viitanen:** Conceptualization, Formal analysis, Writing – review & editing.

Declaration of competing interest

The authors declare that they have no known competing financial interests or personal relationships that could have appeared to influence the work reported in this paper.

Acknowledgements

References

Anderson, J.M., Streitlien, K., Barrett, D.S., Triantafyllou, M.S., 1998. Oscillating foils of high propulsive efficiency. J. Fluid Mech. 360, 41–72.

Beaudoin, N., 2013. Energy Wind Will. Patent US 20130202435 A1.

Belibassakis, K.A., Politis, G.K., 2013. Hydrodynamic performance of flapping wings for augmented ship propulsion in waves. Ocean Eng. 72, 227–240.

Bose, N., 2008. Marine Power Prediction and Propulsors. ISBN-10:0939773651. published by SNAME.

DeLaurier, J.D., Harris, J.M., 1982. experimental study of oscillating wing propulsion. J. Aircraft 19 (5), 368–373.

Johansson, P., Davidson, L., 1995. Modified collocated SIMPLEC algorithm applied to buoyancy-affected turbulent flow using s multi-grid procedure. Numer. Heat Tran. B 28, 39–57.

Katz, J., Plotkin, A., 1991. Low Speed Aerodynamics: from Wing Theory to Panel Methods. McGraw-Hill series in aeronautical and aerospace engineering. ISBN 0-07-050446-6.

Kerwin, J.E., 1978. Chang-sup lee. Prediction of steady and unsteady marine propeller performance by numercial lifting-surface theory. In: Trans. SNAME, Paper No. 8, Annual Meeting.

Krieg, M., Mohseni, K., 2017. Comparison of different methods for estimating energetics related to efficiency on a UUV with cephalopod inspired propulsion. In: Fifth International Symposium on Marine Propulsors smp'17. Espoo, Finland.

Lai, P.S.K., Bose, N., McGregor, R.C., 1993. Wave propulsion from a flexible - armed, rigid - foil propulsor. Mar. Technol. Soc. J. 30 (1), 28–36.

Lighthill, M.J., 1975. Mathematical Bio Fluid Dynamics. Society for Industrial and Applied Mathematics, Philadelphia.

van Manen, J., van Terwisga, T., 1997. A new way of simulating whale tail propulsion. In: Twenty-First Symposium on Naval Hydrodynamics. The National Academies Press, Washington, DC. https://doi.org/10.17226/5870.

Matusiak, J., Rautaheimo, P.P., 25-30 June 2017. Feasibility study on thrust produced by stabilizing fins in waves. In: Proceedings of the 27th International Ocean and Polar Engineering Conference. ISOPE 2017, San Francisco (USA), pp. 1099–1104.

Minaki, H., 2013. Windmill Apparatus for Wind-Powered Generators. Patent WO 2013008672 A1.

Molland, A.F., Turnock, S.R., 2007. Marine Rudders and Control Surfaces: Principles, Data and Design. Butterworth Heineman, p. 414.

Sánchez-Caja, A., Rautaheimo, P., Salminen, E., Siikonen, T., 1999. Computation of the incompressible viscous flow around a tractor thruster using a sliding mesh technique. In: 7th International Conference in Numerical Ship Hydrodynamics. Nantes (France).

Sanchez-Caja, A., Rautaheimo, P., Siikonen, T., Sept. 2000. Simulation of Incompressible Viscous -Flow Around a Ducted Propeller Using a RANS Equation Solver. 23rd Symposium on Naval Hydrodynamics. Val de Reuil, France, pp. 17–22.

Sánchez-Caja, A., González-Adalid, J., Pérez-Sobrino, M., Sipilä, T., 2014. Scale effects on tip loaded propeller performance using a RANSE solver. Ocean Eng. https://doi.org/10.1016/j.oceaneng.2014.04.029i.

Sánchez-Caja, A., Rauti, T., Ramstedt, K., Sipilä, T., May 2017. Numerical investigation of multi-component podded propulsor performance in straight flow. In: 5th International Symposium on Marine Propulsors smp'17. Espoo, Finland.

Sánchez-Caja, A., Martio, J., 2017. On the optimum performance of oscillating foil propulsors. J. Mar. Sci. Technol. 22 (1), 114–124. https://doi.org/10.1007/s00773-016-0397-7.

Sánchez-Caja, A., Martio, J., Saisto, I., Siikonen, T., 2018. A coupled potential–viscous flow approach for the prediction of propeller effective wakes in oblique flow. J. Mar. Sci. Technol. https://doi.org/10.1007/s00773-018-0588-5.

Scherer, J.O., 1968. Experimental and Theoretical Investigation of Large Amplitude Oscillating Foil Propulsion Systems. Report N68-36216. Hydronautics Inc. Laurel, Md.

Smits, A.J., 2016. Underwater flight: hydrodynamics of manta ray swimming invited lecture. In: 31st Symposium on Naval Hydrodynamics.

Steiner, 2002. Apparatus for Generating Fluid Flow. Patent US 6435872 B1.

Syrovy, G.J., 2011. Looped Airfoil Wind Turbine (LAWT). Patent US 20110309634 A1.

Taylor, G.K., Nudds, R.L., Thomas, A.L.R., 2003. Flying and swimming animals cruise at a Strouhal number tuned for high power efficiency. Nature 425, 707–711.

Triantafyllou, M.S., Triantafyllou, G.S., Yue, D.K.P., 2000. Hydrodynamics of fish like swimming. Annu. Rev. Fluid Mech. 32, 33–53.

Triantafyllou, M.S., Techet, A.H., Hover, F.S., 2004. Review of experimental work in biomimetic foils. IEEE J. Ocean. Eng. 29, 585–594.

Vermeiden, J.G., Kooiker, K., Lafeber, F.H., van Terwisga, T., Cerup-Simonsen, B., Folsø, R., August 2012. A systematic experimental study on powering performance of flapping foil propulsors. In: 29th Symposium on Naval Hydrodynamics Gothenburg, pp. 26–31. Sweden.

Vetter, J.W., 2013. Multiorientation, Advanced Vertical Agility Variable-Environment Vehicle. Patent WO 2013/188285 A1.

Wu, T.Y., 1961. Swimming of a waving plate. J. Fluid Mech. 10, 321–344.

Wu, T., 1971. Hydrodynamics of swimming fishes and cetaceans. Adv. Appl. Math 11, 1–63.